Endogenous *KCNE* Subunits Govern Kv2.1 K^+ Channel Activation Kinetics in *Xenopus* Oocyte Studies

Earl Gordon,*† Torsten K. Roepke,*‡ and Geoffrey W. Abbott*‡
*Greenberg Division of Cardiology, Department of Medicine, †Pharmacology Graduate Program, and ‡Department of Pharmacology, Cornell University, Weill Medical College, New York

ABSTRACT Kv2.1 is a voltage-gated potassium (Kv) channel that generates delayed rectifier currents in mammalian heart and brain. The biophysical properties of Kv2.1 and other ion channels have been characterized by functional expression in heterologous systems, and most commonly in *Xenopus laevis* oocytes. A number of previous oocyte-based studies of mammalian potassium channels have revealed expression-level-dependent changes in channel properties, leading to the suggestion that endogenous oocyte factors regulate channel gating. Here, we show that endogenous oocyte potassium channel *KCNE* ancillary subunits xMinK and xMiRP2 slow the activation of oocyte-expressed mammalian Kv2.1 channels two-to-fourfold. This produces a sigmoidal relationship between Kv2.1 current density and activation rate in oocyte-based two-electrode voltage clamp studies. The effect of endogenous xMiRP2 and xMinK on Kv2.1 activation is diluted at high Kv2.1 expression levels, or by RNAi knockdown of either endogenous subunit. RNAi knockdown of both xMiRP2 and xMinK eliminates the correlation between Kv2.1 expression level and activation kinetics. The data demonstrate a molecular basis for expression-level-dependent changes in Kv channel gating observed in heterologous expression studies.

INTRODUCTION

Kv-channels are widely distributed in all excitable cells, where they mediate cellular repolarization (1). Upon membrane depolarization, Kv-channels open to facilitate rapid efflux of K^+ ions through a highly-selective pore (2,3). Kv-channel α-subunits each possess six transmembrane domains (Fig. 1 *A*), and can form functional channels as homotetramers (4) or subfamily-specific heterotetramers (5,6). Kv-current diversity in vivo is generated by a variety of mechanisms, one of which is coassembly of α-subunits with a variety of different ancillary subunits, forming mixed channel complexes with unique function, regulation, and pharmacology (7). One family of ancillary subunits, the MinK-Related Peptides (MiRPs), comprises single transmembrane domain proteins encoded by *KCNE* genes (8,9) (Fig. 1 *A*). MinK and MiRPs coassemble somewhat promiscuously with a range of Kv α-subunits with a variety of functional effects (7). Mutations in *KCNE1* (which encodes MinK) and *KCNE2* (which encodes MiRP1) are associated with inherited and drug-induced cardiac arrhythmia in man (9–13); a *KCNE3* (encoding MiRP2) mutation is associated with familial periodic paralysis (14). Thus, MinK and MiRPs are considered obligate partners in some native channel complexes.

MinK subunits coassemble with KCNQ1 Kv-channel α-subunits to generate the I_{Ks} current in human ventricular myocardium (15,16); MiRP1 coassembles with hERG to form the cardiac I_{Kr} current (9). MiRP2 modulates Kv3.4 α-subunits in skeletal muscle (14), KCNQ1 in the colon (17), and forms complexes with Kv2.1 and with Kv3.1 α-subunits in rat brain (18). Heterologous coexpression studies have shown that MiRP2 is particularly promiscuous, also suppressing hERG currents (17) and slowing the gating of Kv3.2 and Kv3.1-Kv3.2 heteromers (19).

Kv2.1, a mammalian delayed rectifier Kv-channel related to the *Shab* family of *Drosophila melanogaster*, exhibits moderately fast activation and deactivation and slow inactivation (20,21). Kv2.1 channels mediate repolarization of skeletal and cardiac muscles and central and peripheral neurons, regulate tonic firing in sympathetic neurons, and generate the apoptotic response in cortical neurons (22–24).

The *Xenopus laevis* oocyte expression system, coupled with two-electrode voltage-clamp electrophysiology, provides a robust, widely used system for studies of ion channel function, particularly in medium-throughput analyses of ion channel mutations and pharmacology (25). A number of previous studies have shown that heterologously expressed potassium channels in *Xenopus* oocytes exhibit variable functional properties depending upon the amount of α-subunit cRNA injected (26–30). These findings contradict the dogma that ion channels function independently of one another, and prompted speculation that endogenous oocyte factors regulate heterologously-expressed channel function; effects of the endogenous factors are proposed to be diluted at higher α-subunit expression levels. Previously, we identified the *Xenopus* MiRP gene family and showed that endogenous oocyte xMiRP2 suppresses hERG currents heterologously expressed in this system (31). Here, we show using RNA interference (RNAi) that endogenously expressed oocyte xMiRP2 and related protein xMinK dictate Kv2.1 activation kinetics in *Xenopus* oocyte expression studies. The data

Submitted August 11, 2005, and accepted for publication November 21, 2005.
Address reprint requests to Dr. Geoffrey W. Abbott, Greenberg Division of Cardiology, Starr 463, Weill Medical College of Cornell University, 520 E. 70th St., New York, NY, 10021. Tel.: 212-746-6275; Fax: 212-746-7984; E-mail: gwa2001@med.cornell.edu.

0006-3495/06/02/1223/09 $2.00
doi: 10.1529/biophysj.105.072504

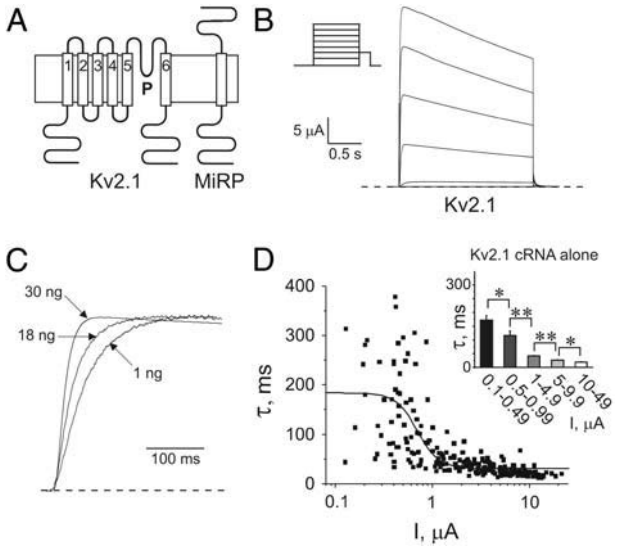

FIGURE 1 Kv2.1 activation kinetics vary with expression level. (*A*) Cartoons showing predicted topologies of Kv2.1 and MinK (or related peptides). (*B*) Exemplar current trace generated from TEVC of oocytes injected with 30 ng Kv2.1 cRNA. Oocytes were held at −80 mV and stepped to voltages between −80 and +60 mV, with a −40 mV tail pulse (protocol, *upper inset*; scale bars, *lower inset*; zero current level, *dashed line*). (*C*) Scaled current at 0 mV for oocytes injected with 1, 18, or 30 ng of Kv2.1 cRNA (as indicated) illustrating current density dependence of activation kinetics (zero current level, *dashed line*). (*D*) Scatter plot of the relationship between the slow component of activation (τ_{slow}) and current density of Kv2.1; oocytes were injected with 1–30 ng Kv2.1 cRNA ($n = 223$ oocytes). Data were fit with a sigmoidal relationship (*solid line*). (*Inset*) Slow component of Kv2.1 activation kinetics versus binned current density for oocytes as in scatter plot. Asterisks indicate statistical significance as determined by one-way ANOVA: single asterisks, $p < 0.05$; double-asterisks, $p < 0.01$. Error bars indicate S.E.

demonstrate for the first time that endogenous potassium channel ancillary subunits in heterologous expression systems can account for expression-level-dependent changes in channel gating, and suggest that previous studies of Kv2.1 function in *Xenopus* oocytes are of mixed Kv2.1-MiRP channel complexes.

MATERIALS AND METHODS

Molecular biology

xMinK and xMiRP2 were cloned from cDNA isolated from RT-PCR from stage V and stage VI *Xenopus laevis* oocytes mRNA as previously described (31). For functional expression in oocytes, cRNA transcripts for xMinK, xMiRP2, hMinK, hMiRP2, and rat Kv2.1 were produced in vitro using the mMessage mMachine transcription kit (Ambion, Austin, TX) as before (31). To avoid dilution errors, all oocytes were first injected with the appropriate α-subunit cRNA, then immediately afterwards injected with modifying β-subunit cRNA transcripts or siRNA oligos.

For RNAi, 500 pg of double-stranded siRNA 21-mer oligos (Dharmacon, Lafayette, CO) corresponding to bases 104–124 of xMiRP2 (top strand 5′-AAGGGAACCACACGGACGCCA-3′) or bases 76–96 of xMinK (top strand 5′-AACUCCACGGCAAUAAAGUCU-3′) were injected into oocytes immediately after injection of α-subunit cRNA as previously described (31,32). For assessment of RNAi gene silencing at the mRNA level, equal amounts of oocytes were injected either with xMiRP2 cRNA, xMiRP2, xMinK, or scrambled control siRNA; and RNA extracted using Trizol (Invitrogen, Carlsbad, CA) the same day as functional experiments were carried out, and on the same batch of oocytes. RNA concentration was measured by spectrophotometry (SmartSpec3000; BioRad, Hercules, CA), and RT-PCR was performed with *Xenopus* β-actin primers (forward, 5′-AAGGAGACAGTCTGTGTGCGTCCA-3′; reverse, 5′-CAACATGATT-TCTGCAAGAGCTCC-3′) to normalize mRNA concentration. Optical density of cDNA samples size-fractionated on a 1% agarose gel and stained with ethidium bromide was measured using a BioRad Fluor-S MultiImager (BioRad). cDNA samples normalized to β-actin cDNA concentration were subsequently amplified using xMinK- or xMiRP2-specific primers and presence of specific cDNAs assessed after size fractionation and ethidium bromide staining on a 1% agarose gel.

Biochemistry

Oocytes were lysed with 150 mM NaCl, 0.2 mM PMSF, 20 mM NaF, 10 mM Na_3VO_4, and 50 mM Tris (pH 7.4), and detergents, 1% NP-40, 1% CHAPS, 1% Triton X-100, and 0.5% SDS. Samples were clarified by two separate centrifugations at 10,000 *g* for 20 min before addition of standard SDS-PAGE loading buffer, and separation by SDS-PAGE on 15% gels. After transfer to PVDF membrane, Western blots were performed with an in-house primary antibody raised by injection into rabbits of a mammalian expression vector expressing full-length hMiRP2; detection was via goat anti-rabbit horseradish peroxidase-coupled secondary antibodies (BioRad) for fluorography. Band intensities for assessment of RNAi efficiency at the protein level were quantified using a BioRad Fluor-S MultiImager (BioRad). Normalization to total protein concentration was not performed, because our previous studies using the Bradford assay showed that normalization to number of oocytes is sufficient to achieve standardized total protein concentration (31).

Electrophysiology

Whole-cell currents in oocytes were recorded 1–2 days post-injection at room temperature by TEVC using an OC-725C Amplifier (Warner Instruments, Hamden, CT), an IBM computer, and pCLAMP8 software (Axon Instruments, Foster City, CA). Bath solution was 4 mM KCl, 96 mM NaCl, 0.7 mM $MgCl_2$, 1 mM $CaCl_2$, and 10 mM HEPES (pH 7.4). In all cases, recordings with a current density below 0.1 μA at 0 mV were discarded to minimize the contribution of endogenous, non-Kv2.1 generated oocyte currents in analyzed data. To eliminate I_{Ks}-like currents generated from interaction of injected xMinK with endogenous xKCNQ1, the I_{Ks}-specific blocker HMR1556 (33–35), generously provided by Aventis Pharmaceuticals (Bridgewater, NJ), was included in the bath medium where appropriate at a concentration of 5 μM. Kv2.1 activation traces were fitted with a double-exponential function. Changes in Kv2.1 activation rate were associated with changes in both the fast and slow components of activation, with no mean significant changes in the relative amplitudes of the two components (not shown). Therefore, for simplicity, scatter plots are of current density versus τ_{slow}; similar effects were observed with equivalent plots using τ_{fast} (not shown). Scatter plots were, where possible, fitted with a logistic dose response function, $y = [A_1–A_2/1 + (x_0/x)^p] + A_2$, where x_0 is the half-maximal effect, and p is the slope factor; coefficient of determination (R^2) was noted to indicate wellness of fit. Scatter plots that did not fit with a logistic dose response function were assumed to show no sigmoidal relationship between current density and activation kinetics, and were instead fit with a straight line, $y = Bx + A$; and values for y intercept (A), slope (B), correlation coefficient (R), standard deviation (SD), and significance level (p) reported (Table 1). Raw data were analyzed using pClamp9 software (Axon Instruments); fitting of plots and statistical analyses (ANOVA) were performed using Excel (MicroSoft, Redmond, WA) and

TABLE 1 Effects of *Xenopus* MinK and MiRP2 on expression level dependence of Kv2.1 activation kinetics

Sigmoidal (logistic) fit	A_1	A_2	x_0	*slope*	*n*	R^2
Kv2.1 cRNA	181.9 ± 16.3	28.0 ± 5.1	0.77 ± 0.10	2.93 ± 0.80	223	0.53
+control siRNA	187.3 ± 9.4	56.8 ± 8.0	2.46 ± 0.28	3.41 ± 1.19	191	0.36
+xMinK siRNA	122.38 ± 7.24	38.8 ± 13.9	2.19 ± 0.44	4.23 ± 2.68	146	0.27
Linear fit	*A*	*B*	*R*	*SD*	*n*	*p*
+xMiRP2 cRNA	148.6 ± 10.6	−36.4 ± 8.2	−0.171	117.0	166	0.048
+xMinK cRNA	266.6 ± 14.7	−70.5 ± 2.6	−0.39	105.5	56	0.0029
+xMiRP2 siRNA	71.6 ± 4.2	−37.8 ± 7.9	−0.45	38.9	95	<0.0001
+xMiRP2/xMinK siRNA	47.1 ± 1.8	−15.2 ± 3.3	−0.50	14.7	68	<0.0001

Scatter plots were fit with a logistic dose response function, $y = [A_1–A_2/1 + (x_0/x)^p] + A_2$, where x_0 is the current at half-maximal effect (μA) and p is the slope factor; R^2 is the coefficient of determination. Scatter plots that did not fit with a logistic dose response were fit with a straight line, $y = Bx + A$; values are also shown for correlation coefficient (R), standard deviation (SD), and significance level (p). In all cases, n = number of oocytes per group.

Origin 6.1 (MicroCal, Northampton, MA) software, with a significance level $p < 0.05$ taken as indicative of significant difference between groups.

RESULTS AND DISCUSSION

Kv2.1 activation is faster at higher current densities

A broad range of Kv2.1 cRNA concentrations were injected—between 1 and 30 ng per oocyte—yielding a range of current densities between 0 and 20 μA at 0 mV membrane potential (Fig. 1, *B–D*). There was a striking correlation between current density and activation kinetics, namely that Kv2.1 activation became faster with higher current densities (Fig. 1, *C* and *D*). The correlation between Kv2.1 activation rate and current density was assessed by fitting activation at 0 mV with a double-exponential function, and plotting the slow component of activation versus corresponding current density for each oocyte ($n = 223$ oocytes).

We hypothesized that there exists in oocytes a finite level of an endogenous moiety that significantly slows Kv2.1 activation at low Kv2.1-expression levels, but the effects of which are diluted as Kv2.1 expression is increased by injecting more Kv2.1 cRNA. This situation has parallels to considerations of fractional occupancy of a finite number of receptors by increasing amounts of a ligand. Thus, the scatter plot was fit with a sigmoidal curve (Fig. 1 *D*, *solid line*) (for values, see Table 1), as would be plotted for effect versus log of ligand concentration for studies of receptor occupancy. Results are also shown using binning of oocytes according to current density (Fig. 1 *D*, *inset*), showing significant differences between the mean activation rates of the different groups.

Overexpressed xMiRP2 eliminates density-dependent changes in Kv2.1 activation kinetics

Kv2.1 coassembles with MiRP2 in mammalian brain to form a slower activating and deactivating channel than Kv2.1 alone (18). Thus, we hypothesized that xMiRP2, which is endogenously expressed in *Xenopus* oocytes, might underlie some of the density-dependent changes in Kv2.1 activation kinetics in oocytes. First, in oocytes injected with 18 ng Kv2.1 cRNA to give high current density, and 3 ng xMiRP2 cRNA, heterologously overexpressed xMiRP2 was found to reduce Kv2.1 current density approximately twofold, and slow the fast and slow components of Kv2.1 activation two-to-fourfold, similar to results previously observed for human MiRP2 with Kv2.1 in Chinese hamster ovary (CHO) cells (18) (Fig. 2, *A–C*). When a large number of oocytes with a range of Kv2.1 cRNA injection levels were studied, it was noticeable that xMiRP2-Kv2.1 currents displayed a relatively wide range of activation kinetics, which may be due to differing efficiencies in coassembly between oocytes, or perhaps that xMiRP2 introduces additional regulatory sites into the channel complex (Fig. 2 *D*). Nevertheless, the scatter plot for xMiRP2-Kv2.1 currents could not be fit with a sigmoidal curve and instead displayed a shallow linear relationship (Fig. 2 *D*, *solid line*, $n = 166$ oocytes; see values in Table 1). This best-fit straight line corresponded very well to the initial part of the sigmoidal curve generated from expression of Kv2.1 alone (Fig. 2 *D*, *dashed line*), corresponding to low levels of Kv2.1 expression. Evaluation of the data using binning according to current density (Fig. 2 *D*, *inset*) showed that differences in activation rate between groups were much less significant than observed in the absence of overexpressed xMiRP2 (Fig. 1 *D*, *inset*).

Endogenous xMiRP2 contributes to current density-dependent changes in Kv2.1 activation kinetics

RNA interference (RNAi) was next employed to knock down endogenous xMiRP2 expression to directly assess its contribution to density-dependent changes in Kv2.1 activation kinetics, as previously employed to assess interaction with hERG (31). RNA was isolated from noninjected oocytes or oocytes injected with siRNA for xMiRP2, scrambled siRNA, or cRNA for xMiRP2. RT-PCR to produce cDNA was followed by normalization of samples to *Xenopus* β-actin cDNA concentration (Fig. 3 *A*, *upper panel*). Next,

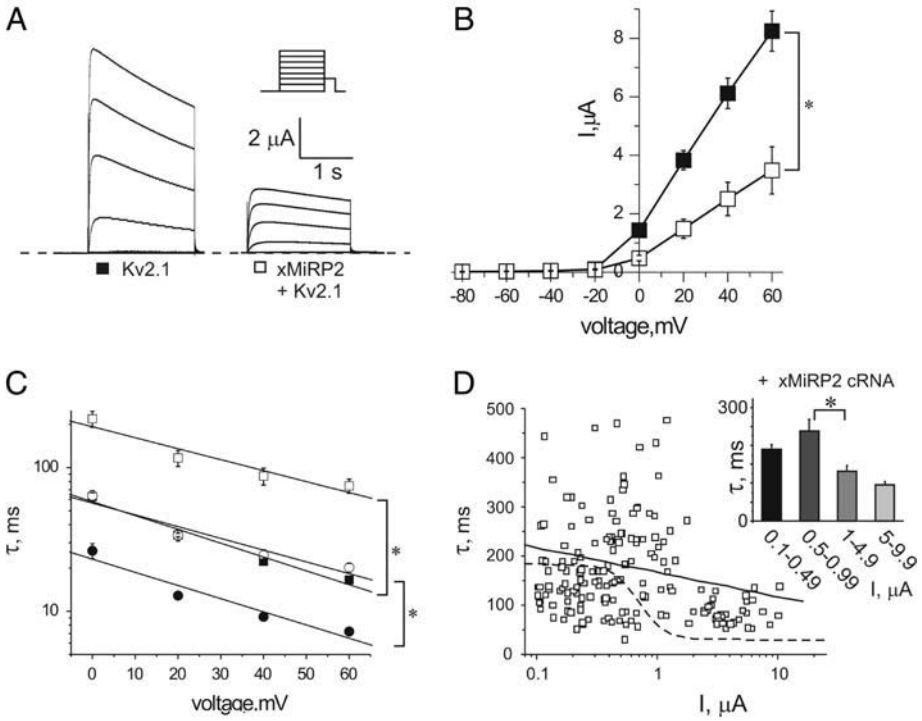

FIGURE 2 Overexpressed xMiRP2 slows Kv2.1 activation. (*A*) Exemplar current traces generated from TEVC of oocytes injected with 18 ng Kv2.1 or coinjected with 3-ng xMiRP2 and 18-ng Kv2.1 cRNA. Oocytes were held at −80 mV and stepped to voltages between −80 and +60 mV, with a −40 mV tail pulse (protocol, *upper inset*; zero current level, *dashed line*). (*B*) Mean current-voltage relationships from traces in *A* for Kv2.1 (*solid squares*) or xMiRP2-Kv2.1 (*open squares*) channels in oocytes, $n = 13$–15 oocytes. Error bars indicate mean ± SE. Single asterisk indicates significant difference between groups at 0–60 mV, $p < 0.0005$. (*C*) Time constants for double-exponential fits of activation to peak currents for Kv2.1 (*solid squares*, τ_{slow}; *solid circles*, τ_{fast}) and xMiRP2-Kv2.1 (*open squares*, τ_{slow}; *open circles*, τ_{fast}; $n = 13$–15 oocytes per group). The single asterisk indicates significant difference between groups at all voltages, $p < 0.0001$. (*D*) Scatter plot of the relationship between the slow component of activation (τ_{slow}) and current density for oocytes coinjected with 1–30 ng Kv2.1 cRNA and 3 ng xMiRP2 cRNA ($n = 166$ oocytes). Solid line indicates linear fit for these data. Dashed line indicates the sigmoidal fit for Kv2.1 cRNA alone data from Fig. 1 *D* for comparison. (*Inset*) Slow component of activation kinetics versus binned current density for oocytes as in scatter plot. Asterisk indicates statistical significance as determined by one-way ANOVA, $p < 0.05$.

normalized cDNA samples were probed for xMiRP2 cDNA by PCR using sequence-specific primers (Fig. 3 *A*, *lower panel*). RNAi of endogenous xMiRP2 using xMiRP2-specific siRNA oligos knocked down endogenous xMiRP2 mRNA expression such that a band could no longer be detected whereas injection of xMiRP2 cRNA increased band intensity and control (scrambled) siRNA oligos had no effect on band intensity (Fig. 3 *A*, *lower panel*).

Western blotting using anti-MiRP2 antibodies was used to evaluate the efficiency of xMiRP2 knockdown at the protein level (Fig. 3 *B*). Oocytes injected with xMiRP2 cRNA showed a 1.8-fold increase in xMiRP2 protein, whereas oocytes injected with xMiRP2 siRNA showed a 6.8-fold decrease in endogenous xMiRP2 protein, as assessed by densitometry ($n = 10$ oocytes; similar results were obtained here in a repeat batch, and in a previous study (31)) (Fig. 3 *B*).

Coinjection of Kv2.1 cRNA with scrambled control siRNA oligos produced a current density-activation rate (slow component of double-exponential fit assessed) correlation similar to that observed with Kv2.1 cRNA alone, indicating a lack of nonspecific effects from coinjection of siRNA oligos (Fig. 3 *C*, $n = 191$ oocytes). This scatter plot was fitted with a sigmoidal curve (values in Table 1). Mean activation rates for oocytes binned by current density are shown for comparison (Fig. 3 *C*, *inset*). In contrast, coinjection of xMiRP2-specific siRNA oligos markedly altered the current density-kinetics relationship, resulting in much more rapid Kv2.1 activation across the Kv2.1 cRNA concentration range, and a shallower current density-kinetics relationship (Fig. 3 *D*, $n = 95$ oocytes). This scatter plot did not fit with a sigmoidal function, and instead was fit with a straight line (Fig. 3 *D*, *solid line*; *dashed line* shows sigmoidal fit of control siRNA plot for comparison). Linear fit values are given in Table 1. Much less scatter was observed than previously seen for Kv2.1 alone or Kv2.1 with overexpressed xMiRP2, and mean activation kinetics of binned groups of oocytes (Fig. 3 *D*, *inset*) were faster and less variable than observed with control siRNA or Kv2.1 alone. These data suggest that endogenous xMiRP2 modulates injected Kv2.1 function, and partially underlies density-dependent changes in Kv2.1 activation kinetics.

Endogenous xMinK contributes to current density-dependent changes in Kv2.1 activation kinetics

Because xMiRP2 siRNA did not completely eliminate density-dependent changes in Kv2.1 activation kinetics, we analyzed the effects of a related oocyte-expressed gene, xMinK, on Kv2.1 currents. MinK is best known for its ability to modulate KCNQ1 in mammalian heart, generating the I_{Ks} repolarization current (8,15,16), and interaction of Kv2.1 with MinK has not previously been reported. Studying MinK in the *Xenopus* oocyte expression system presents unique challenges, because MinK upregulates endogenous oocyte xKCNQ1 currents to produce an I_{Ks}-like current (8,16). To

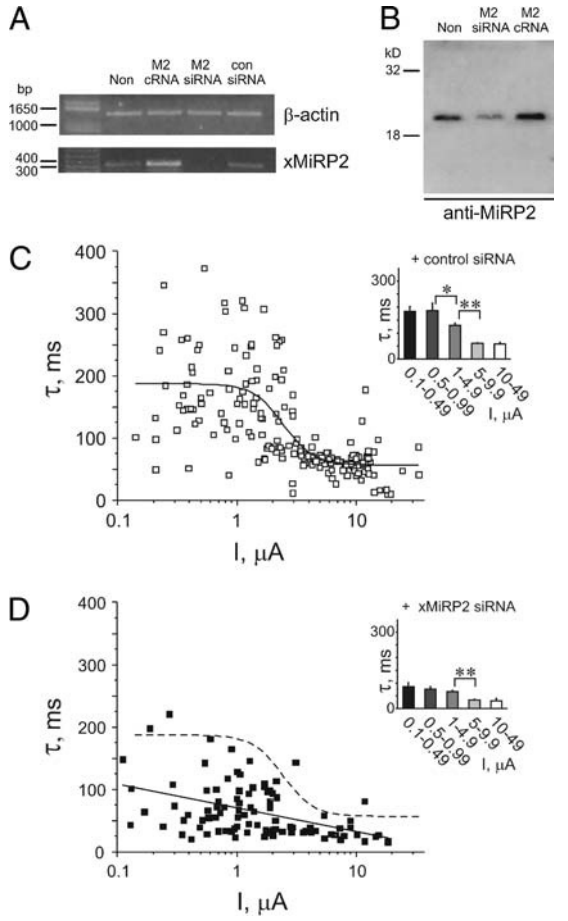

FIGURE 3 Endogenous xMiRP2 modulates Kv2.1 activation kinetics. (*A*) Semiquantitative PCR of cDNA generated by RT-PCR of mRNA isolated from *Xenopus* oocytes. Lanes for both gels (*left* to *right*), uninjected oocytes (*Non*); oocytes injected with 3 ng positive control xMiRP2 cRNA (*M2 cRNA*), 500 pg xMiRP2 siRNA (*M2 siRNA*), or 500 pg scrambled control siRNA (*con siRNA*). (*Upper panel*) *Xenopus* mRNA normalized to endogenous β-actin gene. Bands were generated by PCR using primers specific for *Xenopus* β-actin, and indicate equal amounts of mRNA-generated cDNA loaded in each lane. (*Lower panel*) PCR from cDNA generated from *Xenopus* oocyte mRNA by RT-PCR, and normalized to *Xenopus* β-actin (see above). Bands were generated by PCR using primers specific for *Xenopus* MiRP2 and indicate specific post-transcriptional gene silencing of xMiRP2 by xMiRP2 siRNA. (*B*) Western blot with anti-MiRP2 antibody of lysates from noninjected oocytes (non) or oocytes injected with 500 pg of xMiRP2 siRNA (*M2 siRNA*) or 3 ng xMiRP2 cRNA (*M2 cRNA*). (*C*) Scatter plot of the relationship between the slow component of activation (τ_{slow}) and current density for oocytes coinjected with 1–30 ng Kv2.1 cRNA and 500 pg scrambled control siRNA ($n = 191$ oocytes). (*Inset*) Slow component of activation kinetics versus binned current density for oocytes as in scatter plot. Asterisks indicate statistical significance as determined by one-way ANOVA: single asterisk, $p < 0.05$; double-asterisk, $p < 0.01$. (*D*) Scatter plot of the relationship between the slow component of activation (τ_{slow}) and current density for oocytes coinjected with 1–30 ng Kv2.1 cRNA and 500 pg xMiRP2 siRNA ($n = 95$ oocytes), fit with a linear relationship (*solid line*). Dashed line, sigmoidal fit of data in *C* (control siRNA). (*Inset*) Slow component of activation kinetics versus binned current density for oocytes as in scatter plot. Asterisks indicate statistical significance as determined by one-way ANOVA, $p < 0.01$.

overcome contamination from upregulated xKCNQ1, we included HMR1556—a specific blocker of MinK-KCNQ1 currents (33–35)—in the bath medium, after first confirming that 5 μM HMR1556 completely inhibits xMinK-xKCNQ1 but not xMinK-Kv2.1 currents in oocytes (Fig. 4 *A*). xMinK reduced Kv2.1 current density fourfold (Fig. 4 *B*) and slowed both fast and slow components of Kv2.1 activation two-to-fourfold (Fig. 4 *C*). Overexpression of xMinK also greatly reduced density-dependent changes in Kv2.1 activation rate, eliminating the sigmoidal relationship between current den-

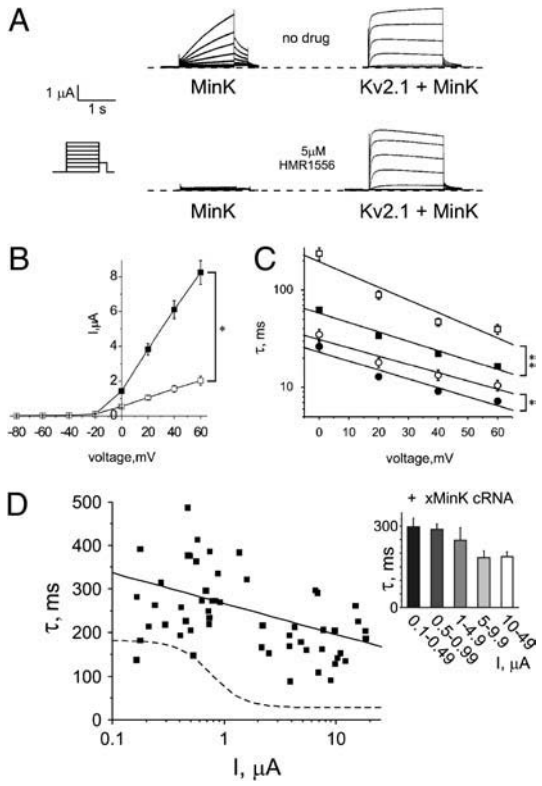

FIGURE 4 Overexpressed xMinK slows Kv2.1 activation. (*A*) Exemplar current traces generated from TEVC of oocytes injected with 3 ng xMinK alone (*left*) or coinjected with 18 ng Kv2.1 cRNA (*right*), in the absence (*upper panel*) or presence (*lower panel*) of HMR1556 (5 μM) in the bath solution. Oocytes were held at -80 mV, then stepped to voltages between -80 mV and $+60$ mV with a -40 mV tail pulse (for protocol, see *inset*). (*B*) Mean current-voltage relationships from traces as in *A* for Kv2.1 (*solid squares*) or xMinK-Kv2.1 (*open squares*) channels, $n = 15$ oocytes per group. Error bars indicate mean $\pm$ SE. Single asterisk indicates significant difference between groups at 0–60 mV, $p < 0.001$. (*C*) Time constants for double-exponential fits of activation to peak currents for Kv2.1 (*solid square*, τ_{slow}; *solid circle*, τ_{fast}; and xMinK-Kv2.1: *open square*, τ_{slow}; *open circle*, τ_{fast}; and $n = 15$ oocytes per group). Error bars indicate SEM. The single asterisk indicates significant difference between groups at 20–60 mV, $p < 0.05$. The double-asterisk indicates significant difference between groups at 0–60 mV, $p < 0.0001$. (*D*) Scatter plot of the relationship between the slow component of activation (τ_{slow}) and current density for oocytes coinjected with 1–30 ng Kv2.1 cRNA and 3 ng xMinK cRNA ($n = 56$ oocytes); solid line is a linear fit of the data. Dashed line, sigmoidal fit of data from Fig. 1 *D* (Kv2.1 cRNA alone). (*Inset*) Slow component of activation kinetics versus binned current density for oocytes as in scatter plot.

sity and activation rate and instead showing a relatively shallow linear correlation (Fig. 4 *D*, *solid line*, $n = 56$ oocytes; *dashed line* shows fit for Kv2.1-alone scatter plot, for comparison) (values in Table 1). Binning of data by current density (Fig. 4 *D*, *inset*) revealed universally slow mean activation kinetics, with no significant differences between groups, showing that xMinK overexpression eliminates density-dependent changes in Kv2.1 activation kinetics.

Next, effects of endogenous xMinK on Kv2.1 activation kinetics were assessed using RNAi knockdown of xMinK. To assess efficiency of xMinK RNAi, RNA was isolated from noninjected oocytes or oocytes injected with siRNA for xMinK, scrambled siRNA, or cRNA for xMinK. RT-PCR to produce cDNA was followed by normalization of samples to *Xenopus* β-actin cDNA concentration (Fig. 5 *A*, *upper panel*). Normalized cDNA samples were probed for xMinK cDNA by PCR using sequence-specific primers (Fig. 5 *A*, *lower panel*). Injection with scrambled control siRNA oligos did not alter band intensity of amplified xMinK cDNA compared to noninjected oocytes, whereas an xMinK band was not observed in cDNA samples obtained from batches of oocytes injected with xMinK siRNA. Injection of 3 ng xMinK cRNA, in contrast, increased band intensity of amplified xMinK cDNA ($n = 10$ oocytes).

Coinjection of xMinK siRNA oligos with Kv2.1 cRNA gave rise to currents with reduced current density-dependence of activation kinetics compared to Kv2.1 alone, assessed by plotting the slow component of Kv2.1 activation versus current density (Fig. 5 *B*). The scatter plot was fitted with a sigmoidal function (*solid line*, $n = 146$ oocytes, values in Table 1), showing overall faster activation at a given current density compared to that observed with control siRNA (*dashed line*). This effect was also apparent from a plot of mean activation kinetics for groups of oocytes binned by current density (Fig. 5 *B*, *inset*). This suggests that endogenous xMinK, like xMiRP2, contributes to density-dependent changes in Kv2.1 activation kinetics.

Endogenous xMiRP2 and xMinK are necessary and sufficient for current density-dependent changes in Kv2.1 activation kinetics

These data raised the possibility that coinjection of specific siRNA oligos for both xMinK and xMiRP2 might further reduce the correlation between Kv2.1 current density and activation kinetics. Coinjection of both xMinK and xMiRP2 siRNA oligos with a range of Kv2.1 cRNA concentrations produced an almost complete loss of the current density-kinetics relationship for Kv2.1, assessed by a scatter plot of the slow component of Kv2.1 activation versus current density (Fig. 5 *C*, $n = 68$ oocytes). This scatter plot could not be fit with a sigmoidal relationship, and therefore was instead fitted with a linear relationship (Fig. 5 *C*, *solid line*). This line had a slope one-half that of the slope for xMiRP2 siRNA alone (*long-dashed line* is the linear fit of xMiRP2-siRNA-

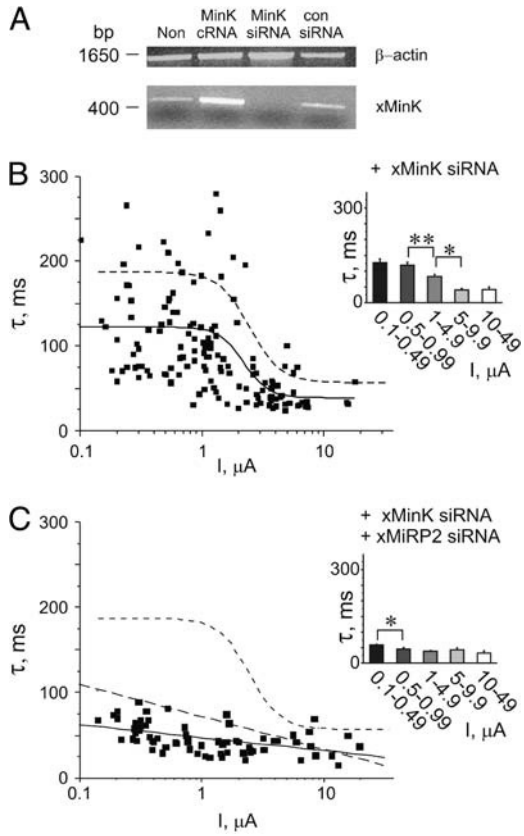

FIGURE 5 Endogenous xMinK and xMiRP2 are necessary and sufficient to explain the correlation between Kv2.1 expression level and activation kinetics. (*A*) Semiquantitative PCR of cDNA generated by RT-PCR of mRNA isolated from *Xenopus* oocytes. Lanes for both gels (*left* to *right*) uninjected oocytes (*Non*); oocytes injected with 3 ng positive control xMinK cRNA (*MinK cRNA*), 500 pg xMinK siRNA (*MinK siRNA*), or 500 pg scrambled control siRNA (*con siRNA*). (*Upper panel*) *Xenopus* mRNA normalized to endogenous β-actin gene. Bands were generated by PCR using primers specific for *Xenopus* β-actin, and indicate equal amounts of mRNA-generated cDNA loaded in each lane. (*Lower panel*) PCR from cDNA generated from *Xenopus* oocyte mRNA by RT-PCR, and normalized to *Xenopus* β-actin (see above). Bands were generated by PCR using primers specific for *Xenopus* MinK and indicate specific post-transcriptional gene silencing of xMinK by xMinK siRNA. (*B*) Scatter plot of the relationship between the slow component of activation (τ_{slow}) and current density for oocytes coinjected with 1–30 ng Kv2.1 cRNA and 500 pg xMinK siRNA ($n = 146$ oocytes). Solid line indicates sigmoidal fit of data. Dashed line, sigmoidal fit of data in Fig. 3 *C* (*control siRNA*). (*Inset*) Slow component of activation kinetics versus binned current density for oocytes as in scatter plot. Asterisks indicate statistical significance as determined by one-way ANOVA: single, $p < 0.05$; double, $p < 0.01$. (*C*) Scatter plot of the relationship between the slow component of activation (τ_{slow}) and current density for oocytes coinjected with 1–30 ng Kv2.1 cRNA, 500 pg xMinK siRNA and 500 pg xMiRP2 siRNA ($n = 68$ oocytes). Solid line indicates linear fit of data. Short-dashed line, sigmoidal fit of data in Fig. 3 *C* (*control siRNA*); long-dashed line, linear fit of data in Fig. 3 *D* (*xMiRP2 siRNA*). (*Inset*) Slow component of activation kinetics versus binned current density for oocytes as in scatter plot. Asterisk indicates statistical significance as determined by one-way ANOVA, $p < 0.05$.

alone data, shown for comparison, from Fig. 3 *D*). The sigmoidal relationship for control siRNA is also shown (*short-dashed line*) for comparison (all values in Table 1). Comparison of activation kinetics for oocytes binned by current density showed relatively fast activation for all groups, with relatively little variation between groups (Fig. 5 *C*, *inset*). These data strongly suggest that endogenous oocyte xMiRP2 and xMinK both regulate the gating kinetics of overexpressed Kv2.1 in oocyte expression experiments, and are the dominant mechanism behind density-dependent changes in Kv2.1 activation kinetics in oocytes.

Endogenous xMiRP2 and xMinK reduce Kv2.1 current density

Analysis of the effects of overexpressed xMiRP2 or xMinK on Kv2.1 showed that either subunit reduces Kv2.1 current density, in addition to effects on gating (Fig. 2, *A* and *B*, and Fig. 4 *B*). These data suggest that Kv2.1 current density should increase nonlinearly with increased cRNA concentration, and also that injection of xMiRP2 or xMinK siRNA should increase Kv2.1 current density at lower Kv2.1 cRNA concentrations. We examined a subset of time-matched recordings of Kv2.1 at various cRNA concentrations performed on the same day with the same batch of oocytes, and found that current density increased in a nonlinear fashion, which could be fitted with a single-exponential function (Fig. 6 *A*). This likely reflects the beginning of a relationship which would adopt a sigmoidal function if injection of much higher amounts of Kv2.1 cRNA were possible, but this was avoided because of potential artifacts due to overwhelming of oocyte translation processes. The nonlinear relationship is consistent with a greater proportional influence of endogenous xMiRPs at lower Kv2.1 cRNA concentrations, with according lower current density at these expression levels due to the partially suppressive effects of endogenous xMinK and xMiRP2.

Similarly, a comparison of Kv2.1 current density at a single cRNA concentration (5 ng) with or without xMiRP2 or xMinK siRNA for time-matched recordings performed on another batch of oocytes showed significantly increased current density with the coinjection of xMiRP2 or xMinK siRNA. This increase in current density was not observed with coinjection of control siRNA (Fig. 6 *B*). These data are again consistent with the partially suppressive effects of either endogenous subunit, and relief of these effects by siRNA knockdown.

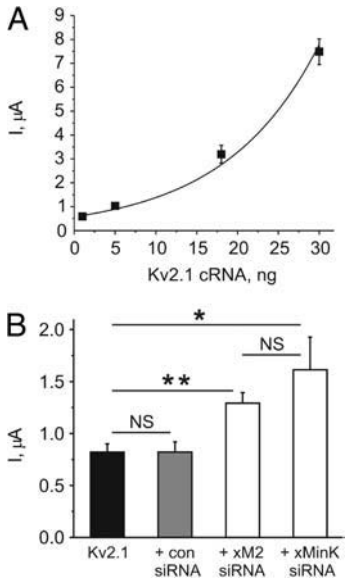

FIGURE 6 Endogenous xMinK and xMiRP2 reduce current density of heterologously expressed Kv2.1. (*A*) Plot of the relationship between the amount of Kv2.1 cRNA injected and current density at 0 mV, for oocytes coinjected with 1–30 ng Kv2.1; $n = 23$–75 oocytes per data point. Solid line indicates single exponential fit of data: $R^2 = 0.97$, $A = 0.58 \pm 0.03$, and $\tau = 11.57863 \pm 0.40$. Error bars indicate mean ± SE. (*B*) Bar graph of the effects of siRNA-coinjection on Kv2.1 current density (24–36 h post-injection) at 0 mV with 5 ng Kv2.1 cRNA injected; $n = 18$–23 oocytes per data set. (*Solid bar*, Kv2.1 alone; *shaded bar*, Kv2.1 + 500 pg control siRNA; *open bar*, labeled ''+ xM2 siRNA'', Kv2.1 + 500 pg xMiRP2 siRNA; and *open bar*, labeled ''+ xMinK siRNA'', Kv2.1 + 500 pg xMinK siRNA.) Asterisks indicate statistical significance as determined by one-way ANOVA: single asterisk, $p < 0.05$; double-asterisk, $p < 0.005$. *NS* = not significant; $p > 0.05$. Error bars indicate mean ± SE.

CONCLUSIONS

The dependence of biophysical properties on expression level has been previously observed for several potassium channel types heterologously expressed in *Xenopus* oocytes. A study of Kv1.2 channels showed that injection of 0.2 ng Kv1.2 cRNA yields very slowly-inactivating current sensitive to dendrotoxin I ($IC_{50} = 2$ nM), whereas injection of 20 ng Kv1.2 cRNA generates a noninactivating current which is much less sensitive to dendrotoxin ($IC_{50} = 200$ nM) (27). Similarly, injection of low levels of Kv1.3 cRNA into *Xenopus* oocytes produced a transient potassium current which was completely inhibited by 10 nM charybdotoxin, whereas high levels of cRNA produced noninactivating current which was hardly sensitive to 10 nM charybdotoxin (28). Further, although low levels of *Shaker* channel ShH4 expression in *Xenopus* oocytes produce a transient, tetraethylammonium-sensitive current, higher expression levels give rise to a slower inactivating current with reduced tetraethylammonium sensitivity (29). Expression level-dependent differences in the properties of Kv channels are also observed with coexpression of two different channel types: coexpression of *Eag* and *Sh* channel subunits in *Xenopus* oocytes leads to accelerated decay of the *Sh* current, but only at higher expression levels (26). These types of effects are not limited to mammalian potassium channels: the inwardly-rectifying KAT1 channel from *Arabidopsis thaliana* showed different gating and sensitivity to external cesium ions depending upon the amount of cRNA injected (30). Some of

the previously described effects have been ascribed to increased clustering of channels at higher expression levels, and may involve interaction with cytoskeletal elements, i.e., with Kv1.3 (28), but this has not been shown in the majority of cases. Here, we demonstrate that expression level-dependent changes in Kv2.1 activation kinetics can be entirely explained by interaction with endogenous xMiRP2 and xMinK.

Previously, the discovery of a family of MiRPs in *Xenopus* oocytes led to the finding that at low levels of hERG expression, endogenous xMiRP2 can suppress hERG currents almost entirely, whereas at higher hERG levels these effects are diluted until at 5 μA, hERG tail currents effects are minimal (31). These followed from previous findings that overexpressed mammalian MiRP2 suppresses hERG currents in oocytes (17). The current finding that endogenous xMiRP2 and xMinK significantly slow the activation kinetics of heterologously expressed Kv2.1 even at relatively high overexpression levels (>1 μA current density at 0 mV) provides the first example of an endogenous potassium channel ancillary subunit, altering potassium channel gating attributes according to α-subunit expression level. We recently found that human MiRP2 slows Kv2.1 activation in CHO cell coexpression studies, and that MiRP2 forms complexes with Kv2.1 in rat brain membranes (18), but interaction of MinK and Kv2.1 has not previously been reported. Using BLAST homology searches, we have not yet found a *Xenopus* variant of MiRP1. Interestingly, in this study we found that neither human MinK nor human MiRP2 have any effects on rat or human Kv2.1 properties in *Xenopus* oocyte coexpression experiments (data not shown), again demonstrating that MiRP-α subunit interaction can show species- and expression-system dependence. However, ongoing studies in our lab show that human variants of MinK and MiRP1, and the rat variant of MinK, modulate Kv2.1 in CHO cell coexpression studies in a similar fashion to effects seen here with *Xenopus* MiRPs and rat Kv2.1 in oocytes (unpublished data). We also previously found that rat MiRP1 but not human MiRP1 modulates Kv3.1 and Kv3.2 α-subunits in CHO cell coexpression studies (19). As yet, the mechanisms for this species- and expression-system dependence have not been elucidated, but they provide another stumbling block in our efforts to understand MiRP physiology.

In summary, the data presented here provide a molecular mechanism for expression-level dependence of Kv2.1 channel properties that may also explain previously-observed density-dependent variation in the biophysical properties of other channels. Although effects of endogenous factors such as MiRPs can be overcome with high expression levels of α-subunits, this is not always feasible, particularly when single-channel analyses are desired; thus in some cases, coinjection of xMiRP-specific siRNA oligos may provide a solution to these potential problems. Further studies will be required to assess whether xMiRPs contribute to pharmacological properties of channels such as Kv2.1 in *Xenopus* oocytes, significant because the oocyte expression system is widely used both in initial electrophysiological studies of ion-channel pharmacology and also in industry for medium throughput screening of pharmacological agents.

Xenopus MiRPs may also explain inconsistencies between studies from different laboratories of the same channel subunits—we previously found that at low levels of hERG expression, endogenous xMiRP2 could reverse the effects of coexpressed human MiRP1 on hERG channels, with MiRP1 increasing hERG currents at low levels presumably by rescue from interaction with endogenous xMiRP2 (31). The presence or absence of particular MiRPs, and the relative expression of various α-subunits compared to available MiRPs within a particular cell in vivo, may provide a physiological mechanism for producing and dynamically regulating the properties of Kv currents, thus explaining variable properties of a particular channel type depending upon the cell type, developmental stage, or disease state studied (36,37).

We thank Ronald Abbott and Gianina Panaghie for thoughtful comments on the manuscript.

G.W.A. is supported by the American Heart Association (grant No. 0235069N) and the National Institutes of Health (grants No. R01 HL079275 and No. RO3 DC07060). We are grateful to Aventis Pharmaceuticals for providing HMR1556.

REFERENCES

1. Hille, B. 2001. Ion Channels of Excitable Membranes. Sinauer Associates, Sunderland, MA.
2. Bezanilla, F. 2000. The voltage sensor in voltage-dependent ion channels. *Physiol. Rev.* 80:555–592.
3. Heginbotham, L., Z. Lu, T. Abramson, and R. MacKinnon. 1994. Mutations in the K^+ channel signature sequence. *Biophys. J.* 66:1061–1067.
4. MacKinnon, R. 1991. Determination of the subunit stoichiometry of a voltage-activated potassium channel. *Nature.* 350:232–235.
5. Li, M., Y. N. Jan, and L. Y. Jan. 1992. Specification of subunit assembly by the hydrophilic amino-terminal domain of the *Shaker* potassium channel. *Science.* 257:1225–1230.
6. Xu, J., W. Yu, Y. N. Jan, L. Y. Jan, and M. Li. 1995. Assembly of voltage-gated potassium channels. Conserved hydrophilic motifs determine subfamily-specific interactions between the α-subunits. *J. Biol. Chem.* 270:24761–24768.
7. McCrossan, Z. A., and G. W. Abbott. 2004. The MinK-related peptides. *Neuropharmacology.* 47:787–821.
8. Takumi, T., H. Ohkubo, and S. Nakanishi. 1988. Cloning of a membrane protein that induces a slow voltage-gated potassium current. *Science.* 242:1042–1045.
9. Abbott, G. W., F. Sesti, I. Splawski, M. E. Buck, M. H. Lehmann, K. W. Timothy, M. T. Keating, and S. A. Goldstein. 1999. MiRP1 forms I_{Kr} potassium channels with HERG and is associated with cardiac arrhythmia. *Cell.* 97:175–187.
10. Isbrandt, D., P. Friederich, A. Solth, W. Haverkamp, A. Ebneth, M. Borggrefe, H. Funke, K. Sauter, G. Breithardt, O. Pongs, and E. Schulze-Bahr. 2002. Identification and functional characterization of a novel KCNE2 (MiRP1) mutation that alters HERG channel kinetics. *J. Mol. Med.* 80:524–532.

11. Sesti, F., G. W. Abbott, J. Wei, K. T. Murray, S. Saksena, P. J. Schwartz, S. G. Priori, D. M. Roden, A. L. George, Jr., and S. A. Goldstein. 2000. A common polymorphism associated with antibiotic-induced cardiac arrhythmia. *Proc. Natl. Acad. Sci. USA*. 97:10613–10618.
12. Splawski, I., M. Tristani-Firouzi, M. H. Lehmann, M. C. Sanguinetti, and M. T. Keating. 1997. Mutations in the hMinK gene cause long QT syndrome and suppress IKs function. *Nat. Genet*. 17:338–340.
13. Tyson, J., L. Tranebjaerg, S. Bellman, C. Wren, J. F. Taylor, J. Bathen, B. Aslaksen, S. J. Sorland, O. Lund, S. Malcolm, M. Pembrey, S. Bhattacharya, and M. Bitner-Glindzicz. 1997. I_{sK} and KvLQT1: mutation in either of the two subunits of the slow component of the delayed rectifier potassium channel can cause Jervell and Lange-Nielsen syndrome. *Hum. Mol. Genet*. 6:2179–2185.
14. Abbott, G. W., M. H. Butler, S. Bendahhou, M. C. Dalakas, L. J. Ptacek, and S. A. Goldstein. 2001. MiRP2 forms potassium channels in skeletal muscle with Kv3.4 and is associated with periodic paralysis. *Cell*. 104:217–231.
15. Barhanin, J., F. Lesage, E. Guillemare, M. Fink, M. Lazdunski, and G. Romey. 1996. K_VLQT1 and I_{sK} (minK) proteins associate to form the I_{Ks} cardiac potassium current. *Nature*. 384:78–80.
16. Sanguinetti, M. C., M. E. Curran, A. Zou, J. Shen, P. S. Spector, D. L. Atkinson, and M. T. Keating. 1996. Coassembly of K_VLQT1 and minK (I_{sK}) proteins to form cardiac I_{Ks} potassium channel. *Nature*. 384:80–83.
17. Schroeder, B. C., S. Waldegger, S. Fehr, M. Bleich, R. Warth, R. Greger, and T. J. Jentsch. 2000. A constitutively open potassium channel formed by KCNQ1 and KCNE3. *Nature*. 403:196–199.
18. McCrossan, Z. A., A. Lewis, G. Panaghie, P. N. Jordan, D. J. Christini, D. J. Lerner, and G. W. Abbott. 2003. MinK-related peptide 2 modulates Kv2.1 and Kv3.1 potassium channels in mammalian brain. *J. Neurosci*. 23:8077–8091.
19. Lewis, A., Z. A. McCrossan, and G. W. Abbott. 2004. MinK, MiRP1 and MiRP2 diversify Kv3.1 and Kv3.2 potassium channel gating. *J. Biol. Chem*. 279:2884–2892.
20. Frech, G. C., A. M. VanDongen, G. Schuster, A. M. Brown, and R. H. Joho. 1989. A novel potassium channel with delayed rectifier properties isolated from rat brain by expression cloning. *Nature*. 340:642–645.
21. Klemic, K. G., C. C. Shieh, G. E. Kirsch, and S. W. Jones. 1998. Inactivation of Kv2.1 potassium channels. *Biophys. J*. 74:1779–1789.
22. Malin, S. A., and J. M. Nerbonne. 2002. Delayed rectifier K^+ currents, IK, are encoded by Kv2 α-subunits and regulate tonic firing in mammalian sympathetic neurons. *J. Neurosci*. 22:10094–10105.
23. Nerbonne, J. M. 2000. Molecular basis of functional voltage-gated K^+ channel diversity in the mammalian myocardium. *J. Physiol*. 525: 285–298.
24. Pal, S., K. A. Hartnett, J. M. Nerbonne, E. S. Levitan, and E. Aizenman. 2003. Mediation of neuronal apoptosis by Kv2.1-encoded potassium channels. *J. Neurosci*. 23:4798–4802.
25. Wagner, C. A., B. Friedrich, I. Setiawan, F. Lang, and S. Broer. 2000. The use of *Xenopus laevis* oocytes for the functional characterization of heterologously expressed membrane proteins. *Cell. Physiol. Biochem*. 10:1–12.
26. Chen, M. L., T. Hoshi, and C. F. Wu. 2000. Sh and Eag K^+ channel subunit interaction in frog oocytes depends on level and time of expression. *Biophys. J*. 79:1358–1368.
27. Guillemare, E., E. Honore, L. Pradier, F. Lesage, H. Schweitz, B. Attali, J. Barhanin, and M. Lazdunski. 1992. Effects of the level of mRNA expression on biophysical properties, sensitivity to neurotoxins, and regulation of the brain delayed-rectifier K^+ channels Kv1.2. *Biochemistry*. 31:12463–12468.
28. Honore, E., B. Attali, G. Romey, F. Lesage, J. Barhanin, and M. Lazdunski. 1992. Different types of K^+ channel current are generated by different levels of a single mRNA. *EMBO J*. 11:2465–2471.
29. Moran, O., W. Schreibmayer, L. Weigl, N. Dascal, and I. Lotan. 1992. Level of expression controls modes of gating of a K^+ channel. *FEBS Lett*. 302:21–25.
30. Very, A. A., C. Bosseux, F. Gaymard, H. Sentenac, and J. B. Thibaud. 1994. Level of expression in *Xenopus* oocytes affects some characteristics of a plant inward-rectifying voltage-gated K^+ channel. *Pflugers Arch*. 428:422–424.
31. Anantharam, A., A. Lewis, G. Panaghie, E. Gordon, Z. A. McCrossan, D. J. Lerner, and G. W. Abbott. 2003. RNA interference reveals that endogenous *Xenopus* MinK-related peptides govern mammalian K^+ channel function in oocyte expression studies. *J. Biol. Chem*. 278:11739–11745.
32. Gordon, E., and G. W. Abbott. 2004. Gene Silencing by RNA Interference: Technology and Application. M. Sohail, editor. CRC Press, Boca Raton, FL.
33. Gerlach, U., J. Brendel, H. J. Lang, E. F. Paulus, K. Weidmann, A. Bruggemann, A. E. Busch, H. Suessbrich, M. Bleich, and R. Greger. 2001. Synthesis and activity of novel and selective I_{Ks}-channel blockers. *J. Med. Chem*. 44:3831–3837.
34. Gogelein, H., A. Bruggemann, U. Gerlach, J. Brendel, and A. E. Busch. 2000. Inhibition of I_{Ks} channels by HMR-1556. *Naunyn Schmiedebergs Arch. Pharmacol*. 362:480–488.
35. Hartmann, R., U. Gerlach, and R. Klinke. 2002. Ototoxic side-effects of the I_{Ks}-channel blocker HMR-1556. *Hear. Res*. 172:145–150.
36. Lundquist, A. L., L. J. Manderfield, C. G. Vanoye, C. S. Rogers, B. S. Donahue, P. A. Chang, D. C. Drinkwater, K. T. Murray, and A. L. George, Jr. 2005. Expression of multiple KCNE genes in human heart may enable variable modulation of I_{Ks}. *J. Mol. Cell. Cardiol*. 38:277–287.
37. Park, K. H., L. Hernandez, S. Q. Cai, Y. Wang, and F. Sesti. 2005. A family of K^+ channel ancillary subunits regulate taste sensitivity in *Caenorhabditis elegans*. *J. Biol. Chem*. 280:21893–21899.